

# Short-Baseline $\bar{\nu}_\mu \rightarrow \bar{\nu}_e$ Oscillations

Carlo Giunti\*

*INFN, Sezione di Torino, Via P. Giuria 1, I-10125 Torino, Italy*

Marco Laveder†

*Dipartimento di Fisica “G. Galilei”, Università di Padova, and INFN,  
Sezione di Padova, Via F. Marzolo 8, I-35131 Padova, Italy*

(Dated: October 26, 2010)

We analyze the recent results of the MiniBooNE short-baseline experiment on  $\bar{\nu}_\mu \rightarrow \bar{\nu}_e$  oscillations in a minimal model-independent framework of antineutrino mixing in conjunction with the positive LSND signal and the negative KARMEN measurements. We show that the data of the three short-baseline  $\bar{\nu}_\mu \rightarrow \bar{\nu}_e$  experiments are compatible. Taking into account also the model-independent constraints due to the limits on short-baseline  $\bar{\nu}_e$  disappearance obtained in reactor antineutrino experiments, we find that the favored region of the effective oscillation parameters lies within  $2 \times 10^{-3} \lesssim \sin^2 2\vartheta \lesssim 5 \times 10^{-2}$  and  $0.2 \lesssim \Delta m^2 \lesssim 2 \text{ eV}^2$ .

PACS numbers: 14.60.Pq, 14.60.Lm, 14.60.St

## I. INTRODUCTION

The MiniBooNE collaboration [1] recently reported the observation of a signal of short-baseline  $\bar{\nu}_\mu \rightarrow \bar{\nu}_e$  transitions compatible with that observed in the LSND experiment [2]. The agreement of the MiniBooNE and LSND signals in favor of neutrino oscillations is remarkable, because the two experiments observed the signal of  $\bar{\nu}_\mu \rightarrow \bar{\nu}_e$  transitions at different source-detector distances and different neutrino energy ranges. Since only the ratio of distance and energy is similar in the two experiments and neutrino oscillations depend just on this ratio (see Refs. [3–10]), the neutrino oscillation explanation of the two signals is strongly favored. On the other hand, the MiniBooNE collaboration did not observe any signal of short-baseline  $\nu_\mu \rightarrow \nu_e$  transitions [11] compatible with the MiniBooNE and LSND signals of  $\bar{\nu}_\mu \rightarrow \bar{\nu}_e$  transitions. Therefore, it is possible that the effective parameters which govern neutrino and antineutrino oscillations are different, maybe because of a violation of the CPT symmetry [12–30]. From a phenomenological point of view, it is interesting to consider the neutrino and antineutrino sectors independently, especially in view of possible experimental checks of the short-baseline  $\bar{\nu}_\mu \rightarrow \bar{\nu}_e$  signal [31–34]. In this paper we adopt this point of view and we present the results of a combined fit of the MiniBooNE and LSND antineutrino data in favor of short-baseline  $\bar{\nu}_\mu \rightarrow \bar{\nu}_e$  transitions, together with the constraints imposed by the data of the KARMEN experiment [35] in which the transitions have not been observed. We also take into account the model-independent constraints imposed by the data of reactor  $\bar{\nu}_e$  disappearance experiments.

In the analysis of the data of  $\bar{\nu}_\mu \rightarrow \bar{\nu}_e$  oscillation experiments we consider the simplest case of an effective two-neutrino-like short-baseline oscillation probability, similar to that obtained in the case of four-neutrino mixing (see Refs. [3, 6, 8, 9]),

$$P_{\bar{\nu}_\mu \rightarrow \bar{\nu}_e}(L/E) = \sin^2 2\vartheta \sin^2 \left( \frac{\Delta m^2 L}{4E} \right), \quad (1)$$

where  $\Delta m^2$  is the relevant neutrino squared-mass difference and  $\vartheta$  is the effective mixing angle for  $\bar{\nu}_\mu \rightarrow \bar{\nu}_e$  transitions.

The plan of the paper is as follows. In Sections II and III we present, respectively, the results of the fits of MiniBooNE and LSND antineutrino data, and in Section IV we discuss the results of the combined fit. In Section V we present the results of the fit of KARMEN data and in Section VI we discuss the results of the combined fit of MiniBooNE, LSND and KARMEN data. In Section VII we discuss the implications of the constraints from reactor  $\bar{\nu}_e$  disappearance experiments. Finally, in Section VIII we draw the conclusions.

## II. MINIBOONE

The MiniBooNE collaboration presented recently the results of a search for  $\bar{\nu}_\mu \rightarrow \bar{\nu}_e$  oscillations obtained with a data sample corresponding to  $5.66 \times 10^{20}$  protons on target [1]. The MiniBooNE detector is located at a distance of 541 m from the neutrino source. The neutrino energy spectrum for the oscillation analysis ranges from 475 MeV to 3 GeV. Hence, the ratio  $L/E$  from which the oscillation probability in Eq. (1) depends ranges from 0.18 to 1.14 m/MeV, leading to a sensitivity to  $\bar{\nu}_\mu \rightarrow \bar{\nu}_e$  transitions for  $\Delta m^2 \gtrsim 10^{-1} \text{ eV}^2$  appropriate for checking the signal observed in the LSND experiment [2] (see Section III).

The excess of  $\bar{\nu}_e$ -like events found by the MiniBooNE collaboration agrees with the excess found in the LSND

\* giunti@to.infn.it; also at Department of Theoretical Physics, University of Torino, Italy

† laveder@pd.infn.it

		MB	LS	MB+LS	KA	MB+LS+KA	Re	(MB+LS+KA)+Re
No Osc.	$\chi^2$	21.4	15.0		6.8		51.0	
	NDF	16	5		8		56	
	GoF	0.16	0.010		0.55		0.66	
Osc.	$\chi^2_{\min}$	11.7	1.4	14.6	6.4	25.7	48.5	77.3
	NDF	14	2	18	6	26	54	82
	GoF	0.63	0.51	0.69	0.38	0.48	0.69	0.63
	$\sin^2 2\theta_{\text{bf}}$	0.91	0.0058	0.006	0.0010	1.00	0.042	0.014
	$\Delta m^2_{\text{bf}}$	0.071	8.13	4.57	6.76	0.052	1.86	0.46
PG	$\Delta\chi^2_{\min}$			1.50		6.32		3.02
	NDF			2		4		2
	GoF			0.47		0.18		0.22

TABLE I. Values of  $\chi^2$ , number of degrees of freedom (NDF), goodness-of-fit (GoF) and best-fit values  $\sin^2 2\theta_{\text{bf}}$ ,  $\Delta m^2_{\text{bf}}$  of the oscillation parameters obtained from the fit of various combinations of MiniBooNE (MB), LSND (LS), KARMEN (KA) and reactor Bugey and Chooz (Re) antineutrino data. The first three lines correspond to the case of no oscillations (No Osc.). The following five lines correspond to the case  $\bar{\nu}_\mu \rightarrow \bar{\nu}_e$  oscillations (Osc.). The last three lines give the parameter goodness-of-fit (PG) [36]. The variations of  $\sin^2 2\theta_{\text{bf}}$  and  $\Delta m^2_{\text{bf}}$  depending on the fitted data sets are due to the oscillating character of  $P_{\bar{\nu}_\mu \rightarrow \bar{\nu}_e}$  in Eq. (1).

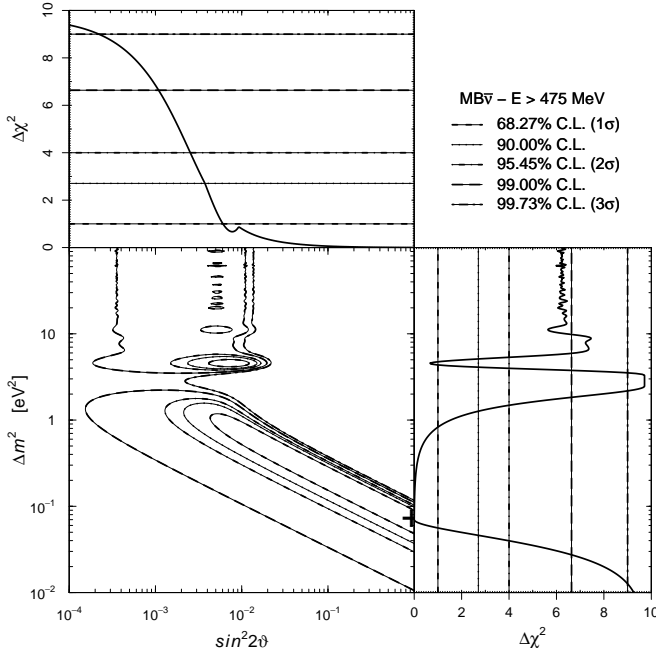


FIG. 1. Allowed regions in the  $\sin^2 2\theta$ - $\Delta m^2$  plane and marginal  $\Delta\chi^2 = \chi^2 - \chi^2_{\min}$ 's for  $\sin^2 2\theta$  and  $\Delta m^2$  obtained from the fit of MiniBooNE (MB) antineutrino data in the energy range  $E > 475$  MeV [1]. The best-fit point is indicated by a cross.

experiment at different source-detector distance and neutrino energy, but similar ratio  $L/E$ . This is a strong indication in favor of the neutrino oscillation explanation of the two signals, analogous to the confirmation of solar neutrino oscillations by the very-long-baseline KamLAND reactor experiment [37] and the confirmation of atmospheric neutrino oscillations by the long-baseline K2K [38] and MINOS [39] accelerator experiments.

In this paper we fit the MiniBooNE data reported in Fig. 1 of Ref. [1]<sup>1</sup> using the method and data given in the MiniBooNE data release in Ref. [40], which are relative to the previous MiniBooNE publication [41] on the search for  $\bar{\nu}_\mu \rightarrow \bar{\nu}_e$  (the MiniBooNE data release relative to Ref. [1] is still not available). We rescaled the signal predicted with the method described in Ref. [40] from the  $3.39 \times 10^{20}$  protons on target corresponding to the sample in Ref. [41] to the  $5.66 \times 10^{20}$  protons on target corresponding to the sample in Ref. [1]. The fractional covariance matrix of systematic uncertainties should be similar in the two data releases. We corrected the statistical part of the covariance matrix by taking into account the different number of background events. In the fit we consider not only the  $\bar{\nu}_e$  MiniBooNE data, but also the  $\bar{\nu}_\mu$  data, which are important because of the correlated uncertainties. Since the  $\bar{\nu}_\mu$  data obtained with  $5.66 \times 10^{20}$  protons on target are not available, we consider the  $\bar{\nu}_\mu$  data given in the MiniBooNE data release in Ref. [40]. The difference is not crucial, because the  $\bar{\nu}_\mu$  data have only an indirect effect on the measurement of the  $\bar{\nu}_\mu \rightarrow \bar{\nu}_e$  signal through the correlated uncertainties.

The results of the least-squares fit of MiniBooNE data are presented in the first column of Tab. I and in Fig. 1. The best-fit values of the oscillation parameters and the allowed regions in the  $\sin^2 2\theta$ - $\Delta m^2$  plane are similar to those obtained by the MiniBooNE collaboration [1]. The goodness-of-fit in the case of no oscillations may seem too high in comparison with that given in Ref. [1] and not sufficient to require oscillations. Since in our calculation we fit both the  $\bar{\nu}_e$  and  $\bar{\nu}_\mu$  data we have 16 degrees of freedom, with  $\chi^2 = 21.4$ . However, most of the  $\chi^2$  is due to the  $\bar{\nu}_e$  data, which have only 8 degrees of freedom,

<sup>1</sup> We would like to thank W.C. Louis for sending us the precise values of the data in Fig. 1 of Ref. [1].

corresponding to the 8 energy bins in Fig. 1 of Ref. [1] for  $E > 475$  MeV. If we restrict the  $\chi^2$  to the six energy bins from 475 to 1300 MeV we have  $\chi^2 = 16.8$ , which is similar to the  $\chi^2 = 18.5$  reported in Ref. [1] for the energy range from 475 to 1250 MeV. Therefore, we agree with Ref. [1] on the opinion that a background-only fit of MiniBooNE data is disfavored.

The first column of Tab. I shows that the oscillation hypothesis fits the MiniBooNE data with a  $\chi^2$  much lower than in the case of no oscillations, improving significantly the goodness-of-fit. The decrease of the  $\chi^2$  with respect to the case of no oscillations is mainly due to the improved fit of the six  $\bar{\nu}_e$  energy bins from 475 to 1300 MeV which give a contribution to  $\chi^2_{\min}$  of 7.2, in approximate agreement with the 8.0 reported in Ref. [1] for the energy range from 475 to 1250 MeV.

From Fig. 1 one can see that, although the best-fit value of  $\sin^2 2\vartheta$  is close to unity, in practice all the allowed straight region in the log-log plot ranging from  $\sin^2 2\vartheta \approx 1$  and  $\Delta m^2 \approx 6 \times 10^{-2} \text{ eV}^2$  to  $\sin^2 2\vartheta \approx 2 \times 10^{-3}$  and  $\Delta m^2 \approx 1 \text{ eV}^2$ , as well as a small area around  $\sin^2 2\vartheta \approx 7 \times 10^{-3}$  and  $\Delta m^2 \approx 5 \text{ eV}^2$ , are equally plausible. This is important, because large values of the effective mixing angle are excluded by the limits on  $\bar{\nu}_e$  disappearance obtained in reactor antineutrino experiments, as explained in Section VII.

### III. LSND

The LSND experiment [2] observed an excess of  $\bar{\nu}_e$  events coming from possible  $\bar{\nu}_\mu \rightarrow \bar{\nu}_e$  transitions in a beam of  $\bar{\nu}_\mu$  produced by  $\mu^+$  decay at rest,

$$\mu^+ \rightarrow e^+ + \nu_e + \bar{\nu}_\mu. \quad (2)$$

The energy spectrum of  $\bar{\nu}_\mu$  is given by (see Ref. [42])

$$\phi_{\bar{\nu}_\mu}(E) \propto E^2 (3 - 4E/m_\mu), \quad (3)$$

for  $E$  smaller than

$$E_{\max} = (m_\mu - m_e)/2 \simeq 52.6 \text{ MeV}. \quad (4)$$

The  $\bar{\nu}_e$ 's produced by  $\bar{\nu}_\mu \rightarrow \bar{\nu}_e$  transitions were detected at an average distance of 30 m through the inverse neutron decay process

$$\bar{\nu}_e + p \rightarrow n + e^+ \quad (5)$$

in a detector consisting of an approximately cylindrical tank 8.3 m long by 5.7 m in diameter, filled with liquid scintillator. Hence, the oscillation distance varied between  $L_{\min} = 25.85 \text{ m}$  and  $L_{\max} = 34.15 \text{ m}$ . The cross section of the detection process in Eq. (5) is (see Refs. [10, 42, 43])

$$\sigma_{\bar{\nu}_e p}(E_e) \propto E_e p_e, \quad (6)$$

where  $E_e$  and  $p_e$  are, respectively, the positron energy and momentum. Neglecting the small recoil energy of the

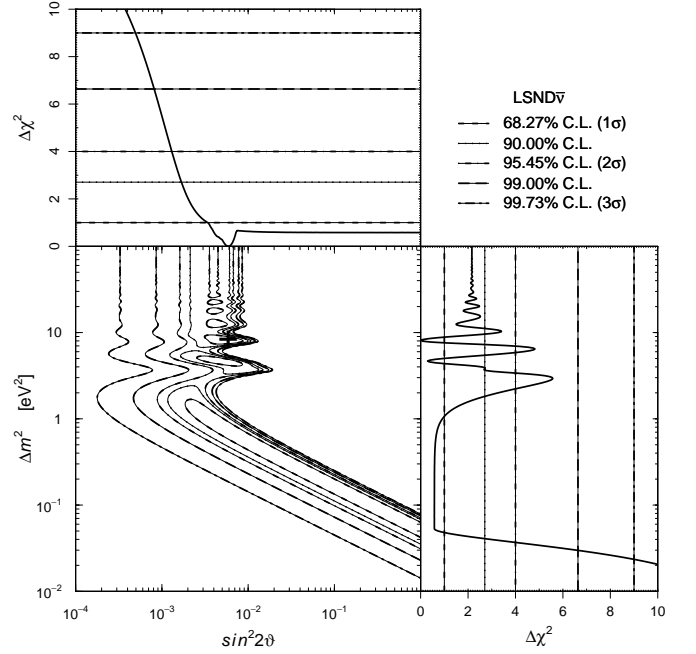


FIG. 2. Allowed regions in the  $\sin^2 2\vartheta$ - $\Delta m^2$  plane and marginal  $\Delta\chi^2$ 's for  $\sin^2 2\vartheta$  and  $\Delta m^2$  obtained from the fit of LSND antineutrino data. The best-fit point is indicated by a cross.

neutron, the positron energy  $E_e$  is related to the neutrino energy  $E$  by

$$E_e = E + m_p - m_n = E - 1.293 \text{ MeV}, \quad (7)$$

where  $m_p$  and  $m_n$  are, respectively, the proton and neutron masses. The neutrino energy threshold is given by

$$E_{\min} = \frac{(m_n + m_e)^2 - m_p^2}{2m_p} = 1.806 \text{ MeV}. \quad (8)$$

The LSND detector had a positron energy resolution which we assume to be Gaussian:

$$R(E'_e, E_e) = \frac{1}{\sqrt{2\pi}\delta_{E_e}} \exp\left(-\frac{(E'_e - E_e)^2}{2\delta_{E_e}^2}\right), \quad (9)$$

with [2]

$$\delta_{E_e} = 3.3 \text{ MeV} \sqrt{\frac{E_e}{50 \text{ MeV}}}. \quad (10)$$

We fit the LSND data in Fig. 16 of Ref. [2], which gives the measured  $\bar{\nu}_e$  events  $N_{\bar{\nu}_e}^i$  in five bins of measured positron energy, their uncertainties  $\delta N_{\bar{\nu}_e}^i$  and the expected number of background events  $B_{\bar{\nu}_e}^i$ . The fit is obtained by minimizing the least-square function

$$\chi^2 = \sum_{i=1}^5 \left( \frac{B_{\bar{\nu}_e}^i + \eta N_{\bar{\nu}_\mu \rightarrow \bar{\nu}_e}^i - N_{\bar{\nu}_e}^i}{\delta N_{\bar{\nu}_e}^i} \right)^2 + \left( \frac{\eta - 1}{\delta\eta} \right)^2. \quad (11)$$

The number  $N_{\bar{\nu}_\mu \rightarrow \bar{\nu}_e}^i$  of  $\bar{\nu}_\mu \rightarrow \bar{\nu}_e$  events in the  $i$ th bin

of measured positron energy between  $E_e^i - \Delta E_e/2$  and  $E_e^i + \Delta E_e/2$  is given by

$$N_{\bar{\nu}_\mu \rightarrow \bar{\nu}_e}^i = N_{\bar{\nu}_\mu \rightarrow \bar{\nu}_e}^0 \frac{\int_{L_{\min}}^{L_{\max}} dL L^{-2} \int_{E_{\min}}^{E_{\max}} dE \phi_{\bar{\nu}_\mu}(E) P_{\bar{\nu}_\mu \rightarrow \bar{\nu}_e}(L/E) \sigma_{\bar{\nu}_e p}(E_e(E)) \int_{E_e^i - \Delta E_e/2}^{E_e^i + \Delta E_e/2} dE'_e R(E'_e, E_e(E))}{\left(\frac{1}{L_{\min}} - \frac{1}{L_{\max}}\right) \int_{E_{\min}}^{E_{\max}} dE \phi_{\bar{\nu}_\mu}(E) \sigma_{\bar{\nu}_e p}(E_e(E)) \int_{E_{\min}}^{E_{\max}} dE'_e R(E'_e, E_e(E))}, \quad (12)$$

where

$$N_{\bar{\nu}_\mu \rightarrow \bar{\nu}_e}^0 = 1.29 \times 10^4 \quad (13)$$

is the number of events expected for 100%  $\bar{\nu}_\mu \rightarrow \bar{\nu}_e$  transmutation in the measured energy range between  $E_e^{\min} = 20$  MeV and  $E_e^{\max} = 60$  MeV. We obtained this number by dividing the  $\bar{\nu}_\mu \rightarrow \bar{\nu}_e$  excess in Fig. 16 of Ref. [2] (34.1 events) by the probability in Tab. XI of Ref. [2] ( $2.64 \times 10^{-3}$ ). The factor  $\eta$  in Eq. (11) is introduced in order to take into account the relative uncertainty of  $N_{\bar{\nu}_\mu \rightarrow \bar{\nu}_e}^0$  [2]:

$$\delta\eta = 0.1. \quad (14)$$

Figure 2 shows the allowed regions in the  $\sin^2 2\vartheta - \Delta m^2$  plane that we obtained from the minimization of  $\chi^2$ , with the best-fit values of the oscillation parameters in the second column of Tab. I. The allowed regions in Fig. 2 are similar to those presented by the LSND collaboration in Ref. [2], with some differences due to the fact that we fitted a data set which is smaller than that used by the LSND collaboration. Similar problems have been encountered in the fits presented in Refs. [44, 45]. In particular, the allowed straight region in the log-log plot ranging from  $\sin^2 2\vartheta \approx 1$  and  $\Delta m^2 \approx 5 \times 10^{-2} \text{ eV}^2$  to  $\sin^2 2\vartheta \approx 10^{-3}$  and  $\Delta m^2 \approx 2 \text{ eV}^2$  and the allowed region at large values of  $\Delta m^2$  are similar to that obtained by the LSND collaboration (see Fig. 27 of Ref. [2]). There is some discrepancy at intermediate values of  $\Delta m^2$ , where we find two favorite regions at  $\Delta m^2 \approx 5 \text{ eV}^2$  and  $\Delta m^2 \approx 8 \text{ eV}^2$ , which however are similar to those obtained in Ref. [45] from a fit similar to ours. Hence, we think that the allowed regions in Fig. 2 are fairly representative of the parameter space allowed by the LSND data.

#### IV. COMBINED FIT OF MINIBOONE AND LSND DATA

Comparing Figs. 1 and 2 one can see that there is a remarkable agreement between the MiniBooNE and the LSND allowed regions in the  $\sin^2 2\vartheta - \Delta m^2$  plane. The results of the combined fit are given in Fig. 3 and in the third column of Tab. I. The excellent parameter goodness-of-fit (PG) [36] of the combined fit quantifies the good compatibility of MiniBooNE and LSND data.

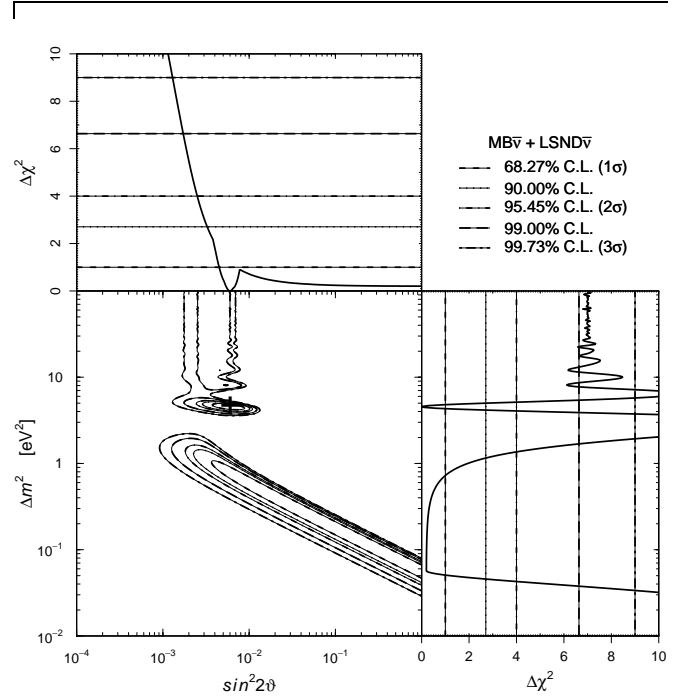


FIG. 3. Allowed regions in the  $\sin^2 2\vartheta - \Delta m^2$  plane and marginal  $\Delta\chi^2$ 's for  $\sin^2 2\vartheta$  and  $\Delta m^2$  obtained from the combined fit of MiniBooNE (MB) and LSND antineutrino data. The best-fit point is indicated by a cross.

From Fig. 3 one can see that the combined fit favors the allowed straight region in the log-log plot ranging from  $\sin^2 2\vartheta \approx 1$  and  $\Delta m^2 \approx 5 \times 10^{-2} \text{ eV}^2$  to  $\sin^2 2\vartheta \approx 2 \times 10^{-3}$  and  $\Delta m^2 \approx 1 \text{ eV}^2$  and an island at  $\sin^2 2\vartheta \approx 6 \times 10^{-3}$  and  $\Delta m^2 \approx 5 \text{ eV}^2$ .

#### V. KARMEN

The KARMEN experiment [35] searched for  $\bar{\nu}_\mu \rightarrow \bar{\nu}_e$  transitions using a beam of  $\bar{\nu}_\mu$  produced by the process of  $\mu^+$  decay at rest in Eq. (2) and detected through the inverse neutron decay process in Eq. (5). Since these processes are the same as those in the LSND experiments, the fit of KARMEN is analogous of that described in Section III for the fit of LSND data. In the KARMEN experiment the oscillation distance varied between  $L_{\min} = 15.935$  m and  $L_{\max} = 19.465$  m. The energy res-

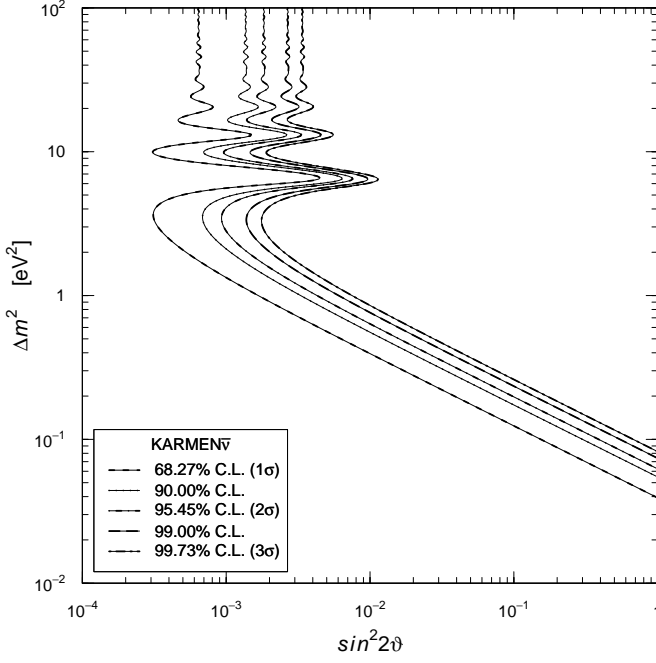


FIG. 4. Exclusion curves in the  $\sin^2 2\theta$ – $\Delta m^2$  plane obtained from the fit of KARMEN antineutrino data.

olution uncertainty was

$$\delta E_e = 0.115 \text{ MeV} \sqrt{\frac{E_e}{\text{MeV}}} . \quad (15)$$

We fit the KARMEN data in Fig. 11b of Ref. [35], which gives the measured  $\bar{\nu}_e$  events  $N_{\bar{\nu}_e}^i$  in nine bins of measured positron energy and the expected number of background events  $B_{\bar{\nu}_e}^i$ . The number of events expected for 100%  $\bar{\nu}_\mu \rightarrow \bar{\nu}_e$  transmutation was

$$N_{\bar{\nu}_\mu \rightarrow \bar{\nu}_e}^0 = 5826 (1 \pm 0.0923) . \quad (16)$$

Since in some energy bins in Fig. 11b of Ref. [35] the number of measured events is zero, we perform the fit by minimizing the least-square function [46]

$$\chi^2 = 2 \sum_{i=1}^9 \left[ B_{\bar{\nu}_e}^i + \eta N_{\bar{\nu}_\mu \rightarrow \bar{\nu}_e}^i - N_{\bar{\nu}_e}^i + N_{\bar{\nu}_e}^i \ln \left( \frac{N_{\bar{\nu}_e}^i}{B_{\bar{\nu}_e}^i + \eta N_{\bar{\nu}_\mu \rightarrow \bar{\nu}_e}^i} \right) \right] + \left( \frac{\eta - 1}{\delta \eta} \right)^2 , \quad (17)$$

with  $\delta \eta = 0.0923$  from Eq. (16).

Figure 4 and the fourth column of Tab. I give the result of the fit of KARMEN data. The best-fit values of the oscillation parameters in Tab. I and the exclusion curves in Fig. 4 are in agreement with those found by the KARMEN collaboration [35], as well as with the results of the fits presented in Refs. [44, 45].

## VI. COMBINED FIT OF MINIBOOONE, LSND AND KARMEN DATA

The results of the combined Fit of MiniBooNE, LSND and KARMEN data on  $\bar{\nu}_\mu \rightarrow \bar{\nu}_e$  oscillations are given in the fifth column of Tab. I and in Fig. 5.

Comparing Figs. 3 and 5 one can see that the inclusion in the analysis of KARMEN data has mainly the effect of disfavoring the regions at  $\Delta m^2 \gtrsim 3 \text{ eV}^2$  allowed by MiniBooNE and LSND data. The straight region in the log-log plot ranging from  $\sin^2 2\theta \approx 1$  and  $\Delta m^2 \approx 5 \times 10^{-2} \text{ eV}^2$  to  $\sin^2 2\theta \approx 10^{-3}$  and  $\Delta m^2 \approx 2 \text{ eV}^2$  allowed by MiniBooNE and LSND data suffers only a small push towards smaller values of  $\sin^2 2\theta$ . The best-fit point lies in this region, close to the large- $\sin^2 2\theta$  and small- $\Delta m^2$  edge. However, from the marginal  $\Delta \chi^2 = \chi^2 - \chi_{\min}^2$ 's

for  $\sin^2 2\theta$  and  $\Delta m^2$  one can see that in practice all the straight region is equally favored. This is important for the compatibility with the reactor limits on  $\sin^2 2\theta$  discussed in the next Section.

## VII. CONSTRAINTS FROM REACTOR $\bar{\nu}_e$ DISAPPEARANCE

Several reactor experiments have searched for the short-baseline disappearance of  $\bar{\nu}_e$ 's (see Refs. [10, 43]), without positive results (apart from the hint discussed in Ref. [47]). Such a lack of short-baseline  $\bar{\nu}_e$  disappearance constrains the probability of all transitions of  $\bar{\nu}_e$  to other flavor antineutrinos and all transitions from other flavor antineutrinos to  $\bar{\nu}_e$ . We are interested in particular in  $\bar{\nu}_\mu \rightarrow \bar{\nu}_e$  oscillations, which are of the second type. The constraint is model-independent and does not require any assumption on the type of mixing and on the number of massive neutrinos, because it follows from simple particle conservation, which is a characteristic of oscillations. In fact, since in neutrino oscillations a  $\bar{\nu}_e$  must come from an antineutrino of some flavor, the sum over the probabilities of transition of any flavor antineutrino into  $\bar{\nu}_e$  is

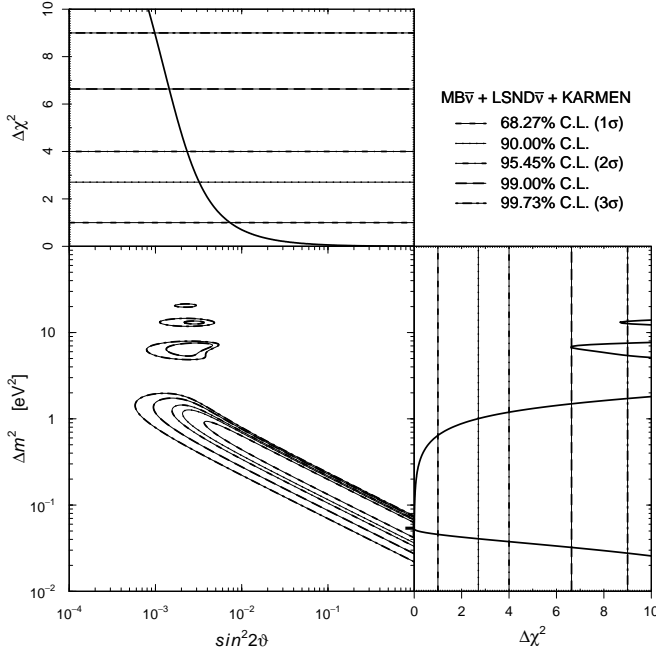


FIG. 5. Allowed regions in the  $\sin^2 2\theta$ – $\Delta m^2$  plane and marginal  $\Delta\chi^2$ 's for  $\sin^2 2\theta$  and  $\Delta m^2$  obtained from the combined fit of MiniBooNE (MB), LSND and KARMEN antineutrino data. The best-fit point is indicated by a cross.

equal to unity:

$$\sum_{\alpha} P_{\bar{\nu}_{\alpha} \rightarrow \bar{\nu}_e} = 1. \quad (18)$$

Then we have the inequality

$$P_{\bar{\nu}_{\mu} \rightarrow \bar{\nu}_e} \leq 1 - P_{\bar{\nu}_e \rightarrow \bar{\nu}_e}. \quad (19)$$

Hence the lower limits obtained in short-baseline reactor antineutrino experiments on  $P_{\bar{\nu}_e \rightarrow \bar{\nu}_e}$  imply model-independent upper limits on  $P_{\bar{\nu}_{\mu} \rightarrow \bar{\nu}_e}$ .

Considering the simplest case of an effective two-neutrino-like short-baseline  $\bar{\nu}_e$  survival probability which is governed by the same  $\Delta m^2$  relevant for the effective short-baseline probability of  $\bar{\nu}_{\mu} \rightarrow \bar{\nu}_e$  transitions in Eq. (1), we have

$$P_{\bar{\nu}_e \rightarrow \bar{\nu}_e}(L/E) = 1 - \sin^2 2\vartheta_{ee} \sin^2 \left( \frac{\Delta m^2 L}{4E} \right), \quad (20)$$

where  $\vartheta_{ee}$  is the effective mixing angle, which can be different from that of  $\bar{\nu}_{\mu} \rightarrow \bar{\nu}_e$  transitions (which we have denoted for simplicity  $\vartheta$ , but could have been called more appropriately  $\vartheta_{e\mu}$ ). In this case, the inequality in Eq. (19) implies

$$\sin^2 2\vartheta \leq \sin^2 2\vartheta_{ee}. \quad (21)$$

Therefore, the exclusion curves obtained in short-baseline reactor antineutrino experiments which place upper limits on the value  $\sin^2 2\vartheta_{ee}$  as a function of  $\Delta m^2$  imply

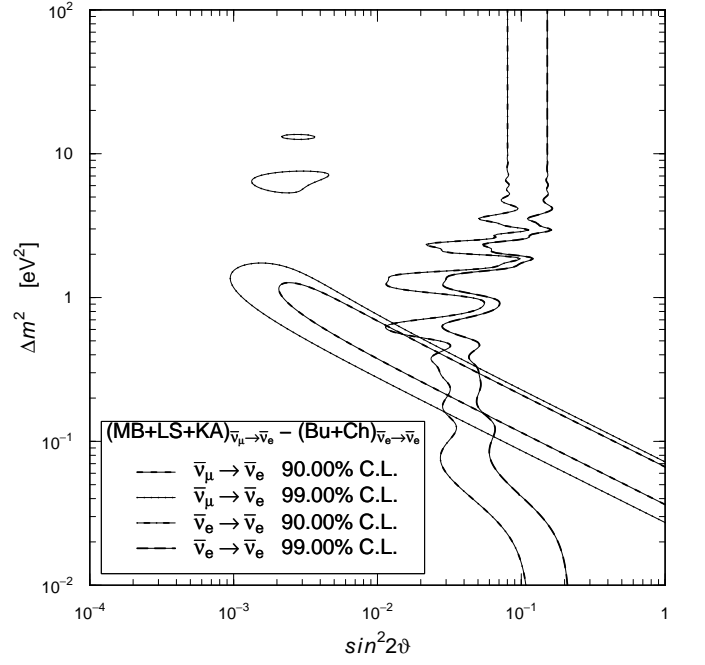


FIG. 6. Superposition of the allowed regions in the  $\sin^2 2\theta$ – $\Delta m^2$  plane obtained from the combined fit of MiniBooNE (MB), LSND (LS) and KARMEN (KA)  $\bar{\nu}_{\mu} \rightarrow \bar{\nu}_e$  data and the exclusion curves obtained from the fit of reactor Bugey (Bu) and Chooz (Ch)  $\bar{\nu}_e \rightarrow \bar{\nu}_e$  data.

model-independent upper limits on the value of  $\sin^2 2\vartheta$  in short-baseline  $\bar{\nu}_{\mu} \rightarrow \bar{\nu}_e$  experiments.

Figure 6 shows a superposition of the 90% and 99% C.L. allowed regions in the  $\sin^2 2\theta$ – $\Delta m^2$  plane obtained from the combined fit of MiniBooNE, LSND and KARMEN  $\bar{\nu}_{\mu} \rightarrow \bar{\nu}_e$  data and the exclusion curves obtained in Ref. [47] from the fit of reactor Bugey [48] and Chooz [49]  $\bar{\nu}_e \rightarrow \bar{\nu}_e$  data, which currently provide the most stringent constraints on short-baseline reactor  $\bar{\nu}_e$  disappearance. The inequality (21) implies that in Fig. 6 the large- $\sin^2 2\theta$  part of the straight region below  $\Delta m^2 \approx 2 \text{ eV}^2$  allowed by the combined fit of MiniBooNE, LSND and KARMEN  $\bar{\nu}_{\mu} \rightarrow \bar{\nu}_e$  data is excluded by the results of reactor antineutrino experiments. Quantitatively, only the parts with  $\sin^2 2\theta \lesssim 3 \times 10^{-2}$  and  $\sin^2 2\theta \lesssim 5 \times 10^{-2}$  are allowed at 90% and 99% C.L., respectively.

The inequality (21) constrains the effective amplitude  $\sin^2 2\vartheta$  of short-baseline  $\bar{\nu}_{\mu} \rightarrow \bar{\nu}_e$  transitions, but does not allow a combined fit of accelerator  $\bar{\nu}_{\mu} \rightarrow \bar{\nu}_e$  data and reactor  $\bar{\nu}_e \rightarrow \bar{\nu}_e$  data. Such a combined fit can be done if the upper limit in Eq. (21) applies, i.e. if the inequality (21) effectively becomes an equality. This is the case if  $P_{\bar{\nu}_{\mu} \rightarrow \bar{\nu}_e} \gg P_{\bar{\nu}_{\alpha} \rightarrow \bar{\nu}_e}$  for  $\alpha \neq e, \mu$ . In the following we consider this interesting possibility, which allows us to combine the accelerator and reactor data in order to find the preferred region in the space of the oscillation parameters which could be explored by future experiments [31–34].

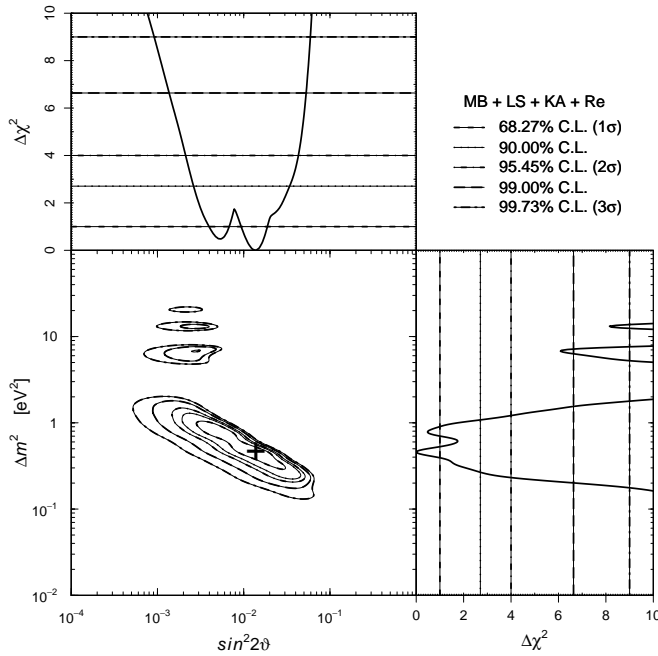


FIG. 7. Allowed regions in the  $\sin^2 2\theta$ – $\Delta m^2$  plane and marginal  $\Delta\chi^2$ 's for  $\sin^2 2\theta$  and  $\Delta m^2$  obtained from the combined fit of MiniBooNE (MB), LSND (LS) and KARMEN (KA)  $\bar{\nu}_\mu \rightarrow \bar{\nu}_e$  data and the exclusion curves obtained from the fit of reactor Bugey and Chooz (Re)  $\bar{\nu}_e \rightarrow \bar{\nu}_e$  data. The best-fit point is indicated by a cross.

Figure 7 and the last column of Tab. I give the results of the combined fit of accelerator MiniBooNE, LSND and KARMEN  $\bar{\nu}_\mu \rightarrow \bar{\nu}_e$  data and reactor Bugey and Chooz  $\bar{\nu}_e \rightarrow \bar{\nu}_e$  data assuming an equality in Eq. (21). The value of the parameter goodness-of-fit in Tab. I shows that the accelerator and reactor data are compatible under the hypothesis of  $\bar{\nu}_\mu \rightarrow \bar{\nu}_e$  oscillations.

From Figure 7 one can see that there is a favorite region at about 95% C.L. around the best-fit point for  $2 \times 10^{-3} \lesssim \sin^2 2\theta \lesssim 5 \times 10^{-2}$  and  $0.2 \lesssim \Delta m^2 \lesssim 2 \text{ eV}^2$ . Larger values of  $\Delta m^2$  are allowed only at more than about 95% C.L. for  $7 \times 10^{-4} \lesssim \sin^2 2\theta \lesssim 5 \times 10^{-3}$ .

## VIII. CONCLUSIONS

We have considered the recent results of the MiniBooNE experiment [1] on short-baseline  $\bar{\nu}_\mu \rightarrow \bar{\nu}_e$  oscillations, which confirm the positive LSND signal [2]. Considering the simplest case of an effective two-neutrino-like short-baseline oscillation probability which depends on only two effective oscillation parameters,  $\sin^2 2\theta$  and  $\Delta m^2$ , we performed a combined fit of MiniBooNE and LSND data in order to find the allowed regions in the parameter space.

We considered also the results of the KARMEN experiment [35], in which  $\bar{\nu}_\mu \rightarrow \bar{\nu}_e$  transitions have not been observed. We have shown that the combined fit of MiniBooNE, LSND and KARMEN data is acceptable and leads to a shift of the region allowed by MiniBooNE and LSND towards small values of  $\sin^2 2\theta$ .

Finally, we have considered the model-independent bound on short-baseline  $\bar{\nu}_\mu \rightarrow \bar{\nu}_e$  implied by the limits on short-baseline  $\bar{\nu}_e$  disappearance obtained in reactor experiments. From a combined fit of accelerator  $\bar{\nu}_\mu \rightarrow \bar{\nu}_e$  data and reactor  $\bar{\nu}_e \rightarrow \bar{\nu}_e$  data we have found that, if the  $\bar{\nu}_\mu \rightarrow \bar{\nu}_e$  channel is dominant over other channels of flavor transitions into  $\bar{\nu}_e$ , the favored region of the effective oscillation parameters lies within  $2 \times 10^{-3} \lesssim \sin^2 2\theta \lesssim 5 \times 10^{-2}$  and  $0.2 \lesssim \Delta m^2 \lesssim 2 \text{ eV}^2$ . This region is interesting for a study of the possibilities to check the LSND and MiniBooNE indication of short-baseline  $\bar{\nu}_\mu \rightarrow \bar{\nu}_e$  oscillations with future experiments [31–34].

- 
- [1] A. A. Aguilar-Arevalo *et al.* (MiniBooNE), (2010), arXiv:1007.1150 [hep-ex].
  - [2] A. Aguilar *et al.* (LSND), Phys. Rev. **D64**, 112007 (2001), arXiv:hep-ex/0104049.
  - [3] S. M. Bilenky, C. Giunti, and W. Grimus, Prog. Part. Nucl. Phys. **43**, 1 (1999), arXiv:hep-ph/9812360.
  - [4] S. M. Bilenky, C. Giunti, J. A. Grifols, and E. Masso, Phys. Rep. **379**, 69 (2003), arXiv:hep-ph/0211462.
  - [5] C. Giunti and M. Laveder, (2003), In “Developments in Quantum Physics – 2004”, p. 197-254, edited by F. Columbus and V. Krasnoholovets, Nova Science, Hauppauge, NY, arXiv:hep-ph/0310238.
  - [6] M. Maltoni, T. Schwetz, M. Tortola, and J. Valle, New J. Phys. **6**, 122 (2004), arXiv:hep-ph/0405172.
  - [7] G. L. Fogli, E. Lisi, A. Marrone, and A. Palazzo, Prog. Part. Nucl. Phys. **57**, 742 (2006), arXiv:hep-ph/0506083.
  - [8] A. Strumia and F. Vissani, (2006), arXiv:hep-ph/0606054.
  - [9] M. C. Gonzalez-Garcia and M. Maltoni, Phys. Rept. **460**, 1 (2008), arXiv:0704.1800 [hep-ph].
  - [10] C. Giunti and C. W. Kim, *Fundamentals of Neutrino Physics and Astrophysics* (Oxford University Press, Oxford, UK, 2007) pp. 1–728.
  - [11] A. A. Aguilar-Arevalo (MiniBooNE), Phys. Rev. Lett. **102**, 101802 (2009), arXiv:0812.2243 [hep-ex].
  - [12] H. Murayama and T. Yanagida, Phys. Lett. **B520**, 263 (2001), arXiv:hep-ph/0010178.
  - [13] G. Barenboim, L. Borissov, J. Lykken, and A. Y. Smirnov, JHEP **10**, 001 (2002), arXiv:hep-ph/0108199.
  - [14] S. M. Bilenky, M. Freund, M. Lindner, T. Ohlsson, and W. Winter, Phys. Rev. **D65**, 073024 (2002), arXiv:hep-ph/0112226.
  - [15] G. Barenboim, L. Borissov, and J. Lykken, Phys. Lett. **B534**, 106 (2002), arXiv:hep-ph/0201080.
  - [16] A. Strumia, Phys. Lett. **B539**, 91 (2002), arXiv:hep-ph/0201134.
  - [17] J. N. Bahcall, V. Barger, and D. Marfatia, Phys. Lett. **B534**, 120 (2002), arXiv:hep-ph/0201211.

- [18] H. Murayama, Phys. Lett. **B597**, 73 (2004), arXiv:hep-ph/0307127.
- [19] V. Barger, D. Marfatia, and K. Whisnant, Phys. Lett. **B576**, 303 (2003), arXiv:hep-ph/0308299.
- [20] H. Minakata and S. Uchinami, Phys. Rev. **D72**, 105007 (2005), arXiv:hep-ph/0505133.
- [21] M. C. Gonzalez-Garcia, M. Maltoni, and T. Schwetz, Phys. Rev. **D68**, 053007 (2003), arXiv:hep-ph/0306226.
- [22] M. Laveder, Nucl. Phys. Proc. Suppl. **168**, 344 (2007), Talk presented at the Workshop on Neutrino Oscillation Physics (NOW 2006), Otranto, Lecce, Italy, 9-16 Sep 2006.
- [23] C. Giunti and M. Laveder, Phys. Rev. **D77**, 093002 (2008), arXiv:0707.4593 [hep-ph].
- [24] S. Antusch and E. Fernandez-Martinez, Phys. Lett. **B665**, 190 (2008), arXiv:0804.2820 [hep-ph].
- [25] C. Giunti and M. Laveder, Phys. Rev. **D80**, 013005 (2009), arXiv:0902.1992 [hep-ph].
- [26] A. D. Dolgov, Phys. Atom. Nucl. **73**, 588 (2010), arXiv:0903.4318 [hep-ph].
- [27] C. Giunti, M. Laveder, and W. Winter, Phys. Rev. **D80**, 073005 (2009), arXiv:0907.5487 [hep-ph].
- [28] G. Barenboim and J. D. Lykken, Phys. Rev. **D80**, 113008 (2009), arXiv:0908.2993 [hep-ph].
- [29] C. Giunti and M. Laveder, Phys. Rev. **D82**, 053005 (2010), arXiv:1005.4599 [hep-ph].
- [30] C. Giunti and M. Laveder, (2010), arXiv:1008.4750 [hep-ph].
- [31] B. Baibussinov *et al.*, (2009), arXiv:0909.0355 [hep-ex].
- [32] I. Stancu *et al.*, (2009), arXiv:0910.2698 [hep-ex].
- [33] S. K. Agarwalla and P. Huber, (2010), arXiv:1007.3228 [hep-ph].
- [34] A. Rubbia, (2010), Talk presented at NEU2012, 27-28 September 2010, CERN, Geneva, Switzerland.
- [35] B. Armbruster *et al.* (KARMEN), Phys. Rev. **D65**, 112001 (2002), arXiv:hep-ex/0203021.
- [36] M. Maltoni and T. Schwetz, Phys. Rev. **D68**, 033020 (2003), arXiv:hep-ph/0304176.
- [37] S. Abe *et al.* (KamLAND), Phys. Rev. Lett. **100**, 221803 (2008), arXiv:0801.4589 [hep-ex].
- [38] M. H. Ahn *et al.* (K2K), Phys. Rev. **D74**, 072003 (2006), arXiv:hep-ex/0606032.
- [39] P. Adamson *et al.* (MINOS), Phys. Rev. Lett. **101**, 131802 (2008), arXiv:0806.2237 [hep-ex].
- [40] A. A. Aguilar-Arevalo *et al.* (MiniBooNE), (2009), URL: [http://www-boone.fnal.gov/for\\_physicists/data\\_release/lowe/](http://www-boone.fnal.gov/for_physicists/data_release/lowe/)
- [41] A. A. Aguilar-Arevalo *et al.* (MiniBooNE), Phys. Rev. Lett. **103**, 111801 (2009), arXiv:0904.1958 [hep-ex].
- [42] M. Fukugita and T. Yanagida, *Physics of neutrinos and applications to astrophysics* (Springer, 2003) pp. 1–593.
- [43] C. Bemporad, G. Gratta, and P. Vogel, Rev. Mod. Phys. **74**, 297 (2002), arXiv:hep-ph/0107277.
- [44] E. D. Church, K. Eitel, G. B. Mills, and M. Steidl, Phys. Rev. **D66**, 013001 (2002), arXiv:hep-ex/0203023.
- [45] M. Sorel, J. Conrad, and M. Shaevitz, Phys. Rev. **D70**, 073004 (2004), arXiv:hep-ph/0305255.
- [46] S. Baker and R. D. Cousins, Nucl. Instrum. Meth. **221**, 437 (1984).
- [47] M. A. Acero, C. Giunti, and M. Laveder, Phys. Rev. **D78**, 073009 (2008), arXiv:0711.4222 [hep-ph].
- [48] B. Achkar *et al.* (Bugey), Nucl. Phys. **B434**, 503 (1995).
- [49] M. Apollonio *et al.* (CHOOZ), Eur. Phys. J. **C27**, 331 (2003), arXiv:hep-ex/0301017.